ACS APPLIED MATERIALS & INTERFACES
Research Article
www.acsami.org

Highly Efficient Photoelectrochemical Hydrogen Generation Using $Zn_xBi_2S_{3+x}$ Sensitized Platelike WO_3 Photoelectrodes

Canjun Liu,[†] Yahui Yang,[‡] Wenzhang Li,*[,†] Jie Li,*[,†] Yaomin Li,[§] Qilin Shi,[†] and Qiyuan Chen[†]

[†]School of Chemistry and Chemical Engineering, Central South University, No. 932 Lushan South Road, Changsha 410083, China
[‡]College of Resources and Environment, Hunan Agricultural University, Changsha 410128, China
[§]Department of Chemistry, University College London, 20 Gordon Street, London WC1H 0AJ, United Kingdom

S *Supporting Information*

ABSTRACT: $Zn_xBi_2S_{3+x}$ sensitized platelike WO_3 photoelectrodes on FTO substrates were for the first time prepared via a sequential ionic layer adsorption reaction (SILAR) process. The samples were characterized by scanning electron microscopy (SEM), transmission electron microscopy (TEM), ultraviolet visible spectrometry (UV−vis), and Raman spectra. The results show that the $Zn_xBi_2S_{3+x}$ quantum dots (QDs) are uniformly coated on the entire surface of WO_3 plates, forming a $WO_3/Zn_xBi_2S_{3+x}$ core/shell structure. The $Zn_xBi_2S_{3+x}/WO_3$ films show a superior ability to capture visible light. High-efficiency photoelectrochemical (PEC) hydrogen generation is demonstrated using the prepared electrodes as photoanodes in a typical three-electrode electrochemical cell. Compared to the Bi_2S_3/WO_3 photoelectrodes, the $Zn_xBi_2S_{3+x}/WO_3$ photoelectrodes exhibit good photostability and excellent PEC activity, and the photocurrent density is up to 7.0 mA cm^{-2} at −0.1 V versus Ag/AgCl under visible light illumination. Investigation of the electron transport properties of the photoelectrodes shows that the introduction of ZnS enhances the photoelectrons' transport rate in the photoelectrode. The high PEC activity demonstrates the potential of the $Zn_xBi_2S_{3+x}/WO_3$ film as an efficient photoelectrode for hydrogen generation.

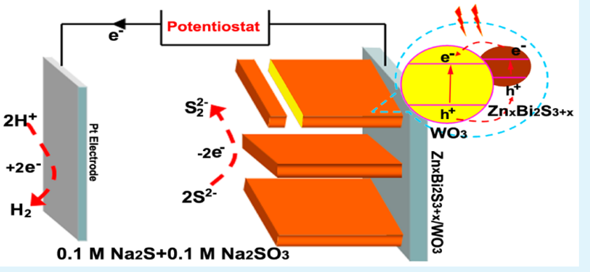

KEYWORDS: *photoelectrochemical, hydrogen generation, WO_3, Bi_2S_3, ZnS*

1. INTRODUCTION

The development of efficient methods for generating renewable and sustainable energy sources is critically important to meet the ever-growing global demand for energy and reduce harmful greenhouse gas emissions from fossil fuels. As one of the most promising methods, photoelectrochemical (PEC) hydrogen generation has attracted extensive attention since the first report on PEC water splitting using TiO_2 photoanodes in 1972.[1−4] Over the past several decades, a variety of nanostructured metal oxides (e.g.TiO_2,[5] ZnO,[6,7] Fe_2O_3,[8] and WO_3[9,10]) as photoanodes have been investigated for PEC hydrogen generation. Among these photoanodes, tungsten trioxide (WO_3) is a promising material because of its high electron mobility, nontoxicity, and low cost.[10,11] More recently, a great deal of attention has been drawn to the fabrication of WO_3 with controlled nanostructures, such as nanoparticles,[12−14] nanoplates,[15−17] nanowires,[18] and nanorods,[19] due to their enhancement in charge separation and transportation. Compared to nanoparticles, low-dimensional WO_3 nanostructure (e.g., nanorods, nanowires, and nanoplates) film can provide a direct pathway for charge transport and an enhancement of charge mobility, which can effectively reduce the recombination of photogenerated electrons and holes.[20−22] Furthermore, a low-dimensional nanostructure usually has the advantage of low reflectance owing to light scattering and trapping over a wide spectrum range, resulting in superior optical absorption properties.[23]

One of the major drawbacks of WO_3 is its large band gap (E_g ≥ 2.6 eV), which means its photocatalytic activity is limited in the near UV region.[24−26] Considerable efforts have been made to expand the spectral response of WO_3 to the visible light region, such as elemental doping (e.g., C,[27] S,[28] and N[24,29,30]) and sensitizing with narrow band gap semiconductors.[31−33] Among various narrow band gap semiconductors, metal sulfide semiconductors (e.g., CdS,[34−36] PbS,[37] In_2S_3[38] and Bi_2S_3[39,40]) have attracted great interest as a sensitizer for PEC hydrogen generation recently. However, their further application is limited by the weak catalytic activity for the hydrogen production and inevitable photocorrosion under the irradiation.[41] ZnS, with a band gap of 3.66 eV, has high photocatalytic activity for H_2 evolution even in the absence of noble metal cocatalysts and good photocorrosion resistance.[42,43] As we know, doping metal sulfides with transition metal elements and coupling metal sulfides with other semiconductors can observably improve their photocatalytic activity and stability.[2,44] Reber's group first reported using

Received: January 27, 2015
Accepted: May 5, 2015
Published: May 5, 2015

DOI: 10.1021/acsami.5b00830
ACS Appl. Mater. Interfaces 2015, 7, 10763−10770

ternary semiconductors $Zn_xCd_{1-x}S$ to form a solid solution between ZnS and CdS improved the photoactivity obviously.[45] Recently, Santra and Kamat, by employing Mn^{2+} doping of CdS, have succeeded in significantly improving QDSC performance and delivered power conversion efficiency of 5.4%.[46] Chidambaram's group demonstrated the synthesis of $Zn_xCd_{1-x}Se$ quantum-dot-sensitized titania nanotube array photoanodes exhibiting excellent PEC properties.[47]

Herein, we have rationally designed and synthesized $Zn_xBi_2S_{3+x}$ QDs using a sequential ionic layer adsorption reaction (SILAR) process. Platelike WO_3 photoelectrodes sensitized with $Zn_xBi_2S_{3+x}$ QDs were fabricated to decompose water into hydrogen. The as-prepared ternary $Zn_xBi_2S_{3+x}$ as sensitizer for WO_3 photoelectrodes show higher PEC activity for H_2 evolution than that of the binary Bi_2S_3. Furthermore, it was found that the ternary photoelectrodes showed a good photostability in an alkaline electrolyte. To the best of our knowledge, this is the first report to synthesize $Zn_xBi_2S_{3+x}/WO_3$ photoelectrodes.

2. EXPERIMENTAL SECTION

2.1. Synthesis and Characterization. All chemicals were analytical grade. WO_3 platelike films were prepared by hydrothermal method according to our previous work.[48,49] A 0.231 g sample of sodium tungsten dehydrate ($Na_2WO_4·2H_2O$) as the tungsten source dissolved in 30 mL of deionized water under constant stirring at room temperature. Then, 10 mL of 3 M HCl was added to the solution, followed by the addition of 0.2 g of ammonium oxalate ($(NH_4)_2C_2O_4$). After several minutes of stirring, 30 mL of deionized water was added into it with continual stirring for 30 min. The as-prepared precursor was transferred into a 100 mL of Teflon-lined stainless autoclave. The FTO substrates with the conducting side facing down were immersed and leaned against the wall of the Teflon-vessel. The hydrothermal synthesis was carried out at 140 °C for 3 h. The as-prepared films were calcined at 450 °C for 1 h. $Zn_xBi_2S_{3+x}$ QDs have been deposited onto WO_3 platelike films by a SILAR method. First, the substrate with WO_3 platelike films were immersed in 20 mM glycol solution of $Bi(NO_3)_3·5H_2O$ and 10 mM $Zn(NO_3)_3$ for 2 min for the adsorption of Bi^{3+} and Zn^{2+} on the platelike WO_3 surface, respectively, and then thoroughly washed with glycol and completely dried at 60−80 °C to remove the solvent. Then it was dipped in 20 mM methanol solution of Na_2S for 2 min, and thoroughly washed with methanol. The S^{2-} reacted with the absorbed Zn^{2+} and Bi^{3+} forming $Zn_xBi_2S_{3+x}$. This two-step dipping procedure was repeated 15 times. We also prepared the pure Bi_2S_3 and $Zn_xBi_2S_{3+x}$ films on FTO substrates by the same process.

The crystalline phase of the electrodes was characterized by X-ray powder diffraction (D/Max2250, Rigaku Corporation, Japan). The surface morphology of the thin films was investigated by scanning electron microscope (SEM, Nova NanoSEM 230). High-resolution transmission electron microscopy (HR-TEM, TECNAI G2 F20, FEI) was operated at 200 kV to observe the microstructure of samples. A spectrophotometer (DR-UVS, Shimadzu 2450 spectrophotometer) was used to record the UV−vis spectra in the range 300−800 nm. Raman spectra were recorded with a LabRAM HR800 Raman analyzer using an excitation laser source of 532 nm wavelength.

2.2. Electrical and Photoelectrochemical Measurements. The photoelectrochemical measurement was carried out in a typical three-electrode electrochemical cell. An Ag/AgCl/satd KCl electrode was employed as the reference electrode, and a platinum foil was used as the counter electrode. All the electrodes were performed in an aqueous solution containing 0.1 M Na_2S and 0.1 M Na_2SO_3 (pH ≈ 9) by an electrochemical analyzer (Zennium, Zahner). A 150 W Xe lamp (CHF-XM35, Beijing Trusttech Co. Ltd.) with a 400 nm cutoff filter to remove UV irradiation was used as the visible light source. The light intensity was adjusted to 100 mW cm^{-2}. Intensity modulated photocurrent spectroscopy (IMPS) were obtained by using a Zahner CIMPS-2 system. A white light lamp emitting diode driven by a PP210 was used as lamp.

3. RESULTS AND DISCUSSION

3.1. XRD, SEM, EDS, XPS, and HR-TEM Analysis. The photographs of the WO_3 film, Bi_2S_3/WO_3 film, and $Zn_xBi_2S_{3+x}/WO_3$ film are shown in Figure 1. Compared with that of the pristine WO_3 film, the color of the Bi_2S_3/WO_3 film and $Zn_xBi_2S_{3+x}/WO_3$ film obviously changed to puce. There is no significant difference between the color of the Bi_2S_3/WO_3 film and the $Zn_xBi_2S_{3+x}/WO_3$ film. However, the XRD patterns of the Bi_2S_3/WO_3 film and the $Zn_xBi_2S_{3+x}/WO_3$ film present the same peaks (Supporting Information Figure S1), corresponding to monoclinic WO_3 (JCPDS 83-0950), and no other obvious peak is observed in all patterns, which is likely due to low Bi_2S_3 and $Zn_xBi_2S_{3+x}$ content. The SEM images observably reveal the high density and uniform vertical alignment of WO_3 plates grown on an FTO substrate (Figure 2). The pristine WO_3 plates have a smooth surface and exhibit an edge length in the range 500 nm to 1.5 μm and a thickness of 50−200 nm (Figure 2a). As shown in Figure 2b−d, the surface morphology of Bi_2S_3/WO_3 and $Zn_xBi_2S_{3+x}/WO_3$ plates is different from that of the pristine WO_3. It is evident that a number of small flakes and dots are aggregated to form a thin shell on the surface of the core WO_3 plates. The local composition of $Zn_xBi_2S_{3+x}/WO_3$ film was analyzed by energy dispersive X-ray spectrometer (EDS). The EDS analysis over the region of the film shows the existence of Zn, Bi, and S in Supporting Information Figure S2. The chemical composition of the $Zn_xBi_2S_{3+x}/WO_3$ film was further characterized by XPS as shown in the Supporting Information Figure S3. The peaks at 163.8 and 158.4 eV are attributed to Bi_{4f} (Supporting Information Figure S3a), and the peaks at 41.4, 37.8 and 35.7 eV are attributed to W^{6+} (Supporting Information Figure S3b). In addition, the peaks at 225.6 eV correspond to S_{2s} (Supporting Information Figure S3c). Importantly, the Zn_{2p} peak can be observed at 1045.1 and 1021.7 eV (Figure 4f), which is in good agreement with the reported work.[47] Figure 3a shows a low-magnification TEM image of the as-prepared $Zn_xBi_2S_{3+x}/WO_3$ plate. The TEM image shows that the $Zn_xBi_2S_{3+x}$ QDs are uniformly distributed on the entire WO_3 plate surface to form a high-quality $WO_3/Zn_xBi_2S_{3+x}$ core/shell nanoplate. The interface between $Zn_xBi_2S_{3+x}$ and WO_3 is shown in the high-magnification TEM of the $Zn_xBi_2S_{3+x}/WO_3$ plate (Supporting Information Figure S4). Figure 3b−e correspond to Bi, Zn, S, and W elemental mappings, respectively, revealing that Bi, S, Zn, and W are homogeneously distributed throughout the WO_3 plate.

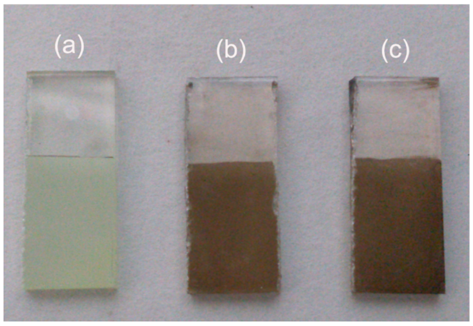

Figure 1. Photographs of the film samples.

DOI: 10.1021/acsami.5b00830
ACS Appl. Mater. Interfaces 2015, 7, 10763−10770

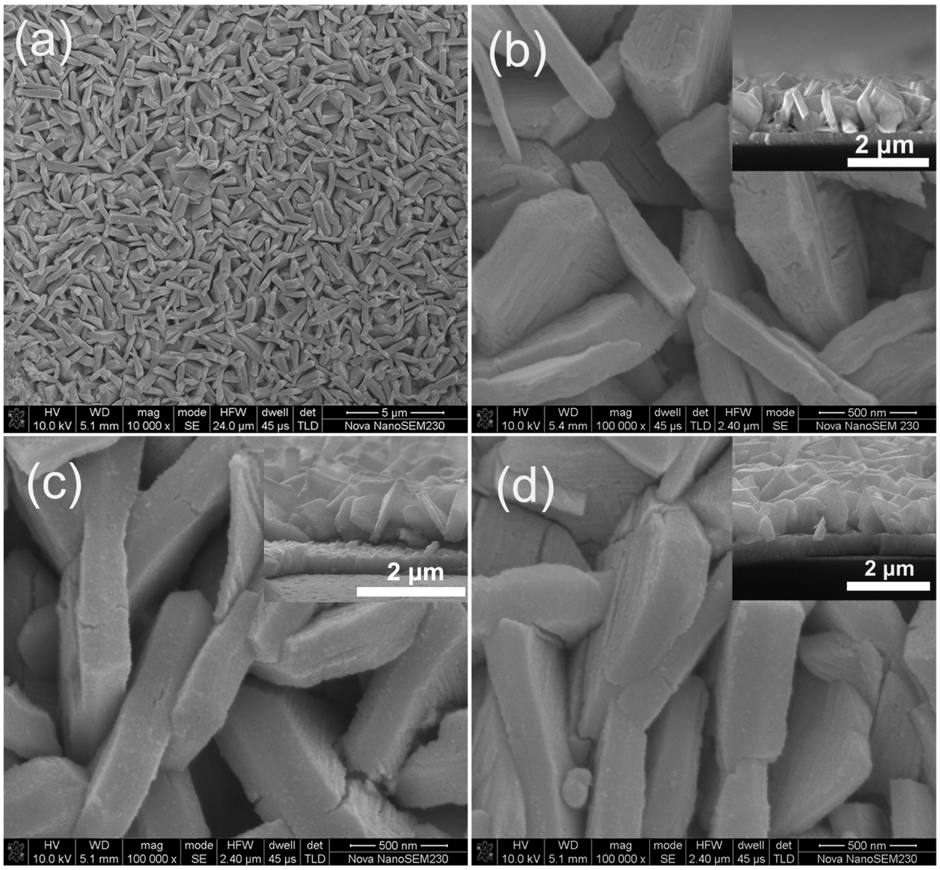

Figure 2. SEM images of (a) WO_3 film at low magnification, (b) WO_3 film, (c) Bi_2S_3/WO_3 film, and (d) $Zn_xBi_2S_{3+x}/WO_3$ film at high magnification.

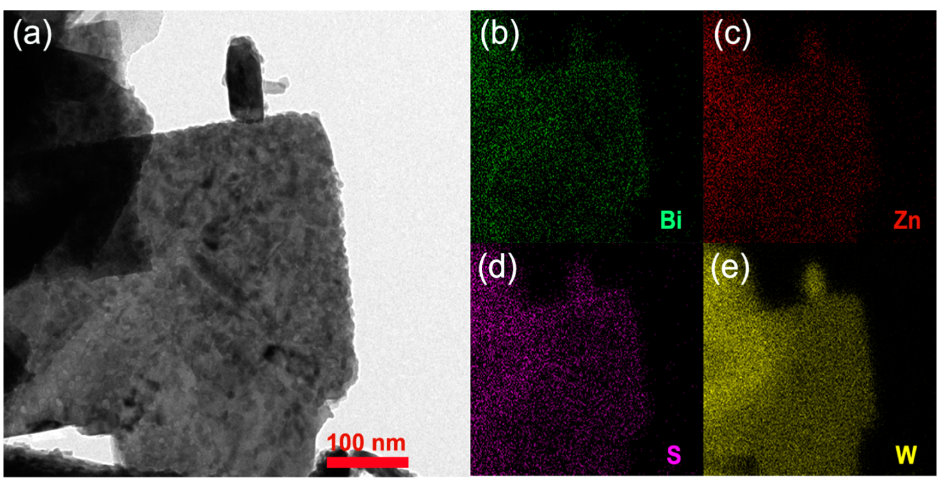

Figure 3. (a) TEM images of $Zn_xBi_2S_{3+x}/WO_3$ plate, and the element distribution maps of (b) Bi, (c) Zn, (d) S, and (e) W on the $Zn_xBi_2S_{3+x}/WO_3$ plate.

3.2. UV−Vis Absorption and Raman Spectra Analysis. The optical behavior of the films was evaluated by UV−vis absorption spectroscopy. Figure 4 illustrates the UV−vis absorption spectra of the WO_3, Bi_2S_3/WO_3, and $Zn_xBi_2S_{3+x}/WO_3$ film. The WO_3 film has a clear absorption edge around 460 nm, which matches well with its indirect band gap energy. For the Bi_2S_3/WO_3 film, it shows a strong absorption intensity around 400−800 nm, which is consistent with its narrow direct band gap. Surprisingly, the absorption intensity of the $Zn_xBi_2S_{3+x}/WO_3$ film shows a little increase in 400−700 nm compared to that of the Bi_2S_3/WO_3 film. As all we know, ZnS is a wide band gap semiconductor (3.5 eV) and can only absorb UV light. It is probably due to the higher absorption coefficient of $Zn_xBi_2S_{3+x}$ for visible light. This result confirms that the as-prepared QDs are a ternary compound, instead of a mixture of ZnS and Bi_2S_3 nanocrystals. To further confirm the nominal composition of the films, Raman spectra of the pure Bi_2S_3 and $Zn_xBi_2S_{3+x}$ films were recorded between 50 and 800 cm^{-1}. As shown in Supporting Information Figure S5, the Bi_2S_3 films show five characteristic peaks at about 70, 97, 186, 236, and 260 cm^{-1}, which is in good agreement with the reported work.[50−52] The $Zn_xBi_2S_{3+x}$ films have similar peaks with no additional

DOI: 10.1021/acsami.5b00830
ACS Appl. Mater. Interfaces 2015, 7, 10763−10770

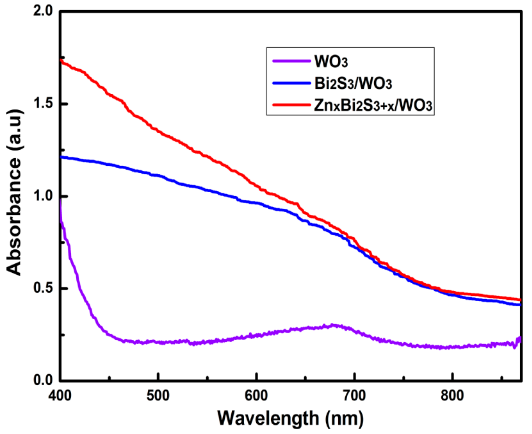

Figure 4. UV−vis absorption spectral of Bi_2S_3/WO_3 film and $Zn_xBi_2S_{3+x}/WO_3$ film.

peaks but a little red shift. It indicates the generation of the ternary compound $Zn_xBi_2S_{3+x}$, instead of a mixture of ZnS and Bi_2S_3.[53]

3.3. Photoelectrochemical Study. The photoelectrochemical measurements were carried out in a three-electrode PEC cell under illumination of AM 1.5 (with UV cutoff). The photocurrent density versus measured potential (I−V) curves of the three photoanodes obtained in the dark and under illumination are shown in Figure 5a. Because the UV light was filtered out from the illumination, the photocurrent density measured for the bare WO_3 electrode is very small (≤0.2 mA). The Bi_2S_3 sensitized WO_3 electrodes exhibit much higher photocurrent than the bare WO_3 electrodes under illumination, which is attributed to the enhanced visible light response. Our

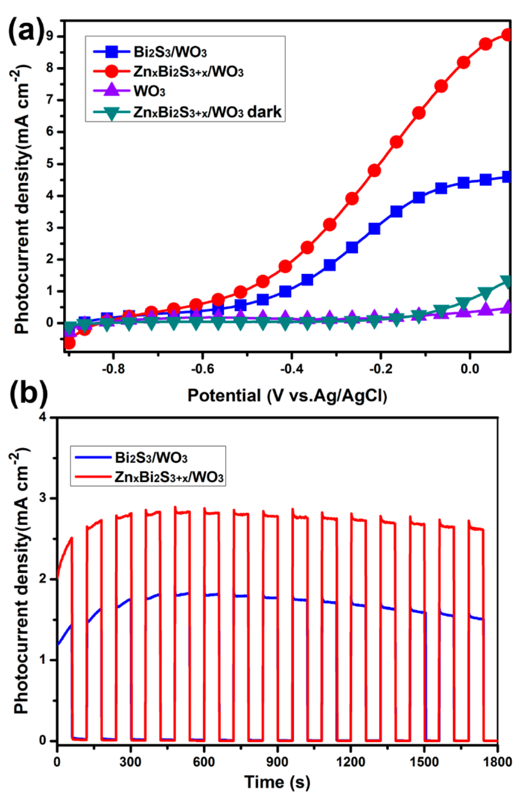

Figure 5. (a) Photocurrent density and (b) photocurrent−time plot of the photoelectrodes.

present result is superior to the recent reports for Bi_2S_3/WO_3 photoelectrodes.[54] Such excellent PEC performance of the Bi_2S_3/WO_3 photoelectrodes can be mainly attributed to their core−shell structures and improved light-harvesting capability.[44] Particularly, the photocurrent density at −0.1 V (vs Ag/AgCl) of the $Zn_xBi_2S_{3+x}/WO_3$ electrode is 7.0 mA cm^{-2}, which is almost 1.8 times higher than that of the Bi_2S_3/WO_3 electrode (3.9 mA cm^{-2}). The high values obtained from the $Zn_xBi_2S_{3+x}/WO_3$ electrode indicate that $Zn_xBi_2S_{3+x}$ is a good candidate material for the promising photosensitizer.

Owing to the importance of the stability of a PEC cell for its practical application, the photoelectrocatalytic stability of the PEC cells was further investigated by performing long-duration photoelectrocatalytic experiments. The experiments were carried out at −0.4 V versus Ag/AgCl under discontinuous illumination. We found that lots of H_2 bubbles were generated on the surface of the Pt electrode upon illumination throughout the entire test. The experimental results are shown in Figure 5b. All the samples show an increasing photocurrent with time in the first 300 s. The I−t curve of the Bi_2S_3/WO_3 electrode shows a decreased photocurrent to some extent in the following 1500 s. Compared to the Bi_2S_3/WO_3 electrode, the photocurrent of the $Zn_xBi_2S_{3+x}/WO_3$ electrode has shown no decrease in the entire test section, and the color has not significantly changed after the stability test. To further verify the stability of the $Zn_xBi_2S_{3+x}/WO_3$ electrode, we also conducted stability tests at −0.1 V versus Ag/AgCl using continuous light illumination with the same group sample. As shown Supporting Information Figure S6, the $Zn_xBi_2S_{3+x}/WO_3$ electrode shows a better photostability and only an approximately 14% decrease in photocurrent after a 7000 s operation under illumination. The absorption spectrum of the electrode after the test is shown in Figure 6a. The absorption intensity for the Bi_2S_3/WO_3 electrode is obviously decreased after a 2 h operation, compared with the absorption spectrum of the electrode before the test. The reproducibility and stable photoresponse for the $Zn_xBi_2S_{3+x}/WO_3$ electrode can be attributed to the formation of the core−shell structure that protects the WO_3 plate from the chemical corrosion in the alkaline electrolyte and good photocorrosion resistance for the ternary metal sulfide alloys.

In addition to photostability, we also measured the H_2 generation at −0.1 V versus Ag/AgCl. The PEC cells have high H_2 yields but poor production of O_2, due to the following chemical reaction: $2S^{2-} + 2h^+ \rightarrow S_2^{2-}$. It can prevent the anodic photocorrosion of Bi_2S_3.[45] The H_2 generation reactions take place at the Pt electrode/electrolyte interface. As shown in Figure 6b, the evolved H_2 at the Pt electrode was collected and analyzed using gas chromatography (GC). The Faradaic efficiency for H_2 production was calculated to be about 88%. The hydrogen evolution rates for Bi_2S_3/WO_3 and $Zn_xBi_2S_{3+x}/WO_3$ electrode are 52.7 and 88.6 μmol cm^{-2} h^{-1}, respectively. The $Zn_xBi_2S_{3+x}/WO_3$ electrode has a higher H_2 generation rate, which is caused by not only the higher photocurrent but also the higher stability of $Zn_xBi_2S_{3+x}/WO_3$ electrode observed for Supporting Information Figure S6.

In order to study the relationship between the PEC activity and the wavelength of the incident light, we performed incident photon-to-current conversion efficiency (IPCE) measurement at an applied voltage of −0.4 V versus Ag/AgCl. The IPCE is expressed as IPCE = $(1240I)/(\lambda J_{light})$, where I is the photocurrent density, λ is the incident light wavelength, and J_{light} is the incident light power density.[34] The IPCE values

DOI: 10.1021/acsami.5b00830
ACS Appl. Mater. Interfaces 2015, 7, 10763−10770

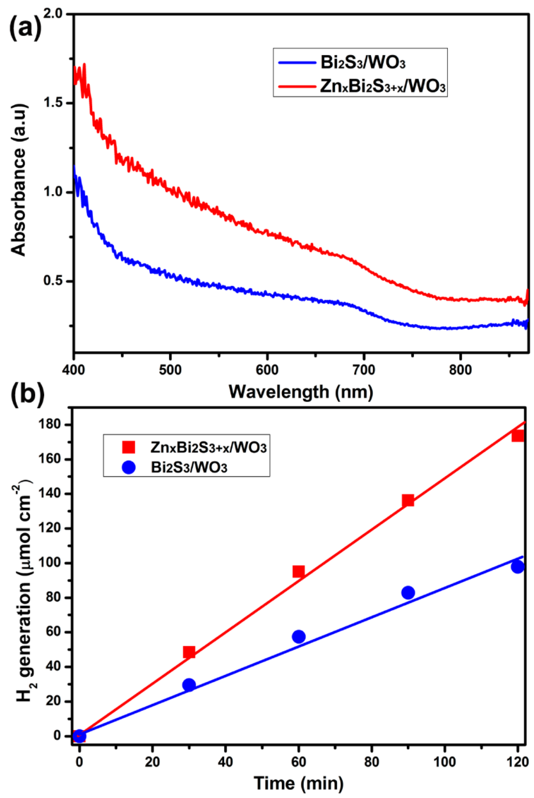

Figure 6. (a) Absorption spectrum of the photoelectrodes after a 2 h operation under illumination. (b) The amounts of evolved H_2 for Bi_2S_3/WO_3 and $Zn_xBi_2S_{3+x}/WO_3$ photoelectrodes at −0.1 V versus Ag/AgCl under continuous light illumination.

obtained for WO_3, Bi_2S_3/WO_3, and $Zn_xBi_2S_{3+x}/WO_3$ electrodes are shown in Figure 7. The pristine WO_3 electrode shows photoactivity only at the wavelength range of ~455 nm due to its large band gap ($E_g \geq 2.6$ eV), with a lower IPCE value of ~16%. In comparison to pristine WO_3 electrode, sensitized WO_3 electrode show substantially enhanced IPCE in the entire testing wavelength region because of the increased light absorption by the QDs. As expected, the IPCE value of

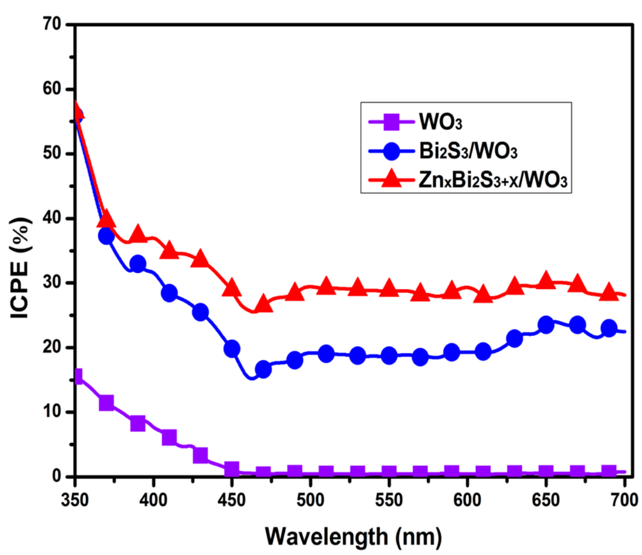

Figure 7. IPCE spectra of WO_3, Bi_2S_3/WO_3, and $Zn_xBi_2S_{3+x}/WO_3$ photoelectrodes.

$Zn_xBi_2S_{3+x}/WO_3$ electrodes is the highest, which is in accordance with the photocurrent results.

To better understand the enhanced PEC property in the $Zn_xBi_2S_{3+x}/WO_3$ photoelectrodes, the electron transport properties were assessed using the electrochemical impedance spectroscopy (EIS). The Nyquist plots were obtained for selected samples under illumination conditions, at the applied potential of −0.4 V versus Ag/AgCl (Figure 8a). One

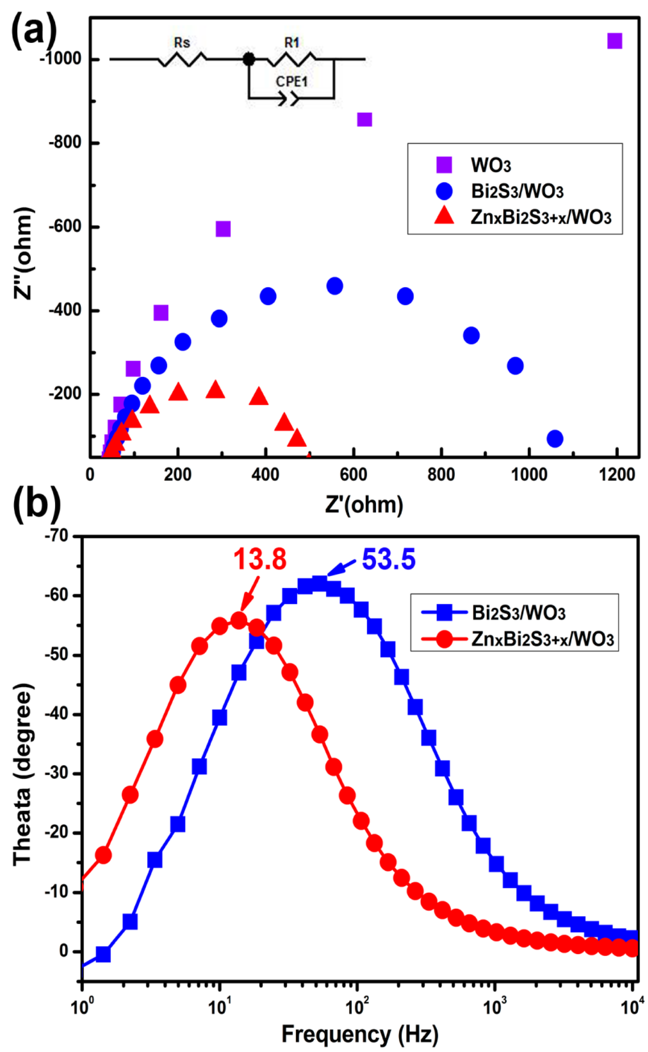

Figure 8. (a) Electrochemical impedance spectra and (b) Bode phase plots of the photoelectrodes.

semicircle is observed for each sample, which is fitted by the equivalent circuit (the inset in Figure 8a) composed of a series resistance (R_S), a charge transfer resistance (R_1), and a capacitance (CPE_1). The R_S corresponds to the sheet resistance of the FTO glass, contact resistance, and wire resistance. The R_1 represents the complex charge transfer resistance at the interface of the semiconductor electrode and the electrolyte.[55] As seen in Table 1, the R_S values of all samples are comparable while the R_1 values are very different. The R_1 values of the $Zn_xBi_2S_{3+x}/WO_3$ photoelectrodes are smaller than that of the Bi_2S_3/WO_3 photoelectrode, which indicates better charge transport property at the interface of the semiconductor electrode and the electrolyte, consistent with the improved PEC property. Similarly, Bode plots in Figure 8b reflect the efficient electron lifetime in Bi_2S_3/WO_3 and $Zn_xBi_2S_{3+x}/WO_3$

DOI: 10.1021/acsami.5b00830
ACS Appl. Mater. Interfaces 2015, 7, 10763−10770

Table 1. Simulated Values of Resistance (Rs) and Charge Transfer Resistance (R_1) of EIS Spectra Calculated by Equivalent Circuit

sample	R_s (Ω cm^2)	R_1 (Ω cm^2)
WO_3	38.08	2499
Bi_2S_3/WO_3	41.89	1019
$Zn_xBi_2S_{3+x}/WO_3$	35.05	470.7

photoelectrodes, respectively. The lifetime (τ_e) can be determined by using the following formula: $\tau_e = 1/2\pi f_{max}$, where the f_{max} is the frequency at which the low-frequency peak appears in the Bode plot.[56] Larger τ_e values indicate that electrons have longer lifetime and faster diffusion rate in the photoelectrode.[57] As presented in Figure 8b, the f_{max} value for Bi_2S_3/WO_3 and $Zn_xBi_2S_{3+x}/WO_3$ is 53.5 and 13.8 Hz, respectively. It suggests that $Zn_xBi_2S_{3+x}/WO_3$ possesses a 4-fold improved lifetime of electrons compared with Bi_2S_3/WO_3. It may be because the introduction of ZnS into Bi_2S_3 results in better photocatalytic activity.

In order to further support the above ideas, we subjected the Bi_2S_3/WO_3 and $Zn_xBi_2S_{3+x}/WO_3$ photoelectrodes to intensity modulated photocurrent spectroscopy (IMPS) analysis. The IMPS is a useful method to investigate semiconductor charge transport properties and is popularly used in electron transport characterization of PEC cells.[12,58,59] During the IMPS measurements, the sample electrodes were biased at −0.4 V (vs Ag/AgCl) and illuminated with a white light emitting diode at 2.19 mW cm^{-2}. Figure 9 shows a complex plane plot of the IMPS

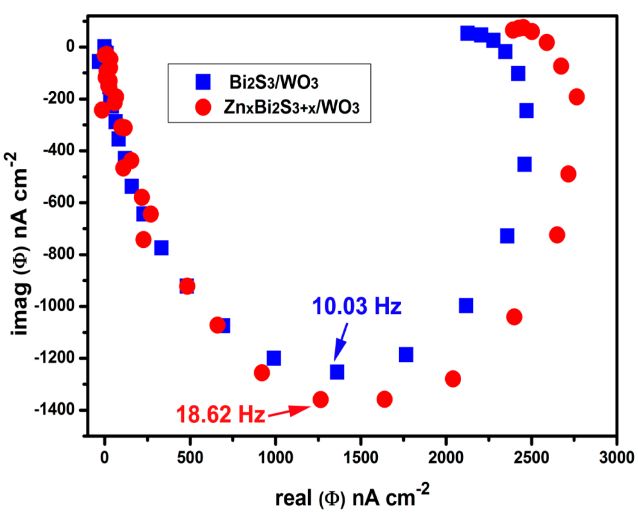

Figure 9. Complex plane plot of the IMPS response of the photoelectrodes.

response in the fourth quadrant. The average transit time (τ_d) of the photogenerated electron can be estimated from the frequency at the apex of the semicircle, given by $\tau_d = (2\pi f_{min})^{-1}$. The average transit times for the Bi_2S_3/WO_3 and $Zn_xBi_2S_{3+x}/WO_3$ photoelectrodes were 15.87 and 8.55 ms, respectively. The results indicate that the $Zn_xBi_2S_{3+x}/WO_3$ photoelectrodes exhibit a higher electron transit rate than the Bi_2S_3/WO_3, supporting the EIS results.

3.4. Mechanism Discussion. To understand how the electrode works for PEC hydrogen production, a model nanostructure of $Zn_xBi_2S_{3+x}/WO_3$ and the possible mechanism are shown in Figure 10. Bi_2S_3 is an n-type semiconductor with a

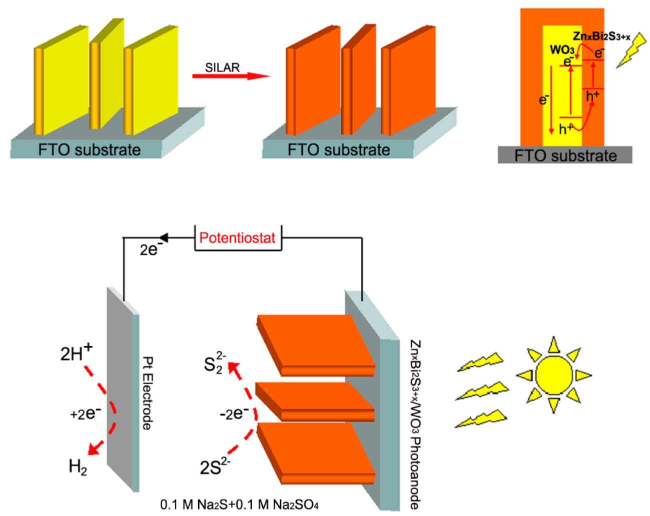

Figure 10. Schematic representation of the formation process of $Zn_xBi_2S_{3+x}/WO_3$ photoelectrodes and the PEC hydrogen production mechanism.

narrow band gap of 1.3 eV and can absorb a large part of visible light up to 800 nm.[60,61] On the contrary, ZnS has a wide band gap (3.5 eV) and can only absorb UV light.[62] ZnS has a more negative conduction band (CB) level (−0.945 V_{NHE}) than that of Bi_2S_3 (0.081 V_{NHE}).[63] When WO_3, ZnS, and Bi_2S_3 are connected together, the energy level differences between ZnS and Bi_2S_3 facilitate the electrons flowing from ZnS (higher level) to Bi_2S_3 (lower level) because of the Fermi level alignment.[53] The redistribution of the electrons between ZnS and Bi_2S_3 results in a downward and upward shift of the band edges, respectively, for ZnS and Bi_2S_3. The band positions of the ternary $Zn_xBi_2S_{3+x}$ locate at an intermediate position between the bands of pure ZnS and pure Bi_2S_3 and can be controlled by varying x value.[45,53] Therefore, the electrons in the VB of $Zn_xBi_2S_{3+x}$ are excited to the CB under visible-light irradiation, and then the excited electrons transfer from the CB of $Zn_xBi_2S_{3+x}$ to the WO_3, because of the lower CB of WO_3 (+0.4 V_{NHE}).[64] The superior PEC performance of the $Zn_xBi_2S_{3+x}/WO_3$ photoelectrodes can be attributed to the following reason. By the introduction of ZnS, the CB level of the ternary $Zn_xBi_2S_{3+x}$ is shifted toward more negative potential values. So the ternary semiconductor has a more positive CB level than that of ZnS but a more negative value than that of Bi_2S_3. It can be supported from the Mott−Schottky results (Supporting Information Figure S7), showing a more negative flat band potential for $Zn_xBi_2S_{3+x}/WO_3$ photoelectrodes. The more negative CB level gives rise to an enhanced charge separation and higher reduction potential of the CB electrons, and results in a more efficient PEC hydrogen production.[44,45] Moreover, ZnS has a good photocorrosion resistance to protect $Zn_xBi_2S_{3+x}$ from photocorrosion. This may be one of the explanations why $Zn_xBi_2S_{3+x}/WO_3$ photoelectrodes keep good stability.

4. CONCLUSION

In this study, $Zn_xBi_2S_{3+x}$ sensitized WO_3 platelike films have been first reported as efficient photoanodes. The $Zn_xBi_2S_{3+x}$ QDs were uniformly deposited by the facile SILAR process on the entire surface of the WO_3 plates to form the core/shell heterostructures. Importantly, the formation of the high-quality core−shell structure protects the WO_3 plate from the chemical

DOI: 10.1021/acsami.5b00830
ACS Appl. Mater. Interfaces 2015, 7, 10763−10770

corrosion in the alkaline electrolyte. The PEC performance of the $Zn_xBi_2S_{3+x}/WO_3$ photoelectrodes is higher than that of Bi_2S_3/WO_3 photoelectrodes under visible light illumination. This may be because the introduction of ZnS improves photocatalytic activity of photoelectrodes for H_2 evolution and photocorrosion resistance. These findings are of great significance for the design of highly efficient photoanodes for hydrogen generation.

■ ASSOCIATED CONTENT

Supporting Information

XRD patterns of Bi_2S_3/WO_3 and $Zn_xBi_2S_{3+x}/WO_3$ film; EDS, XPS, and HRTEM spectra of the $Zn_xBi_2S_{3+x}/WO_3$ film; Raman spectrum, photocurrent−time plot, and Mott−Schottky plots of Bi_2S_3/WO_3 and $Zn_xBi_2S_{3+x}/WO_3$ photoelectrode. The Supporting Information is available free of charge on the ACS Publications website at DOI: 10.1021/acsami.5b00830.

■ AUTHOR INFORMATION

Corresponding Authors

*E-mail: liwenzhang@csu.edu.cn. Phone: +86 731 8887 9616. Fax: +86 731 8887 9616.
*E-mail: lijieliu@csu.edu.cn. Phone: +86 731 8887 9616. Fax: +86 731 8887 9616.

Notes

The authors declare no competing financial interest.

■ ACKNOWLEDGMENTS

This study was supported by the National Nature Science Foundation of China (No. 51474255), the Hunan Provincial Natural Science Foundation of China (No. 13JJ6003), and the Fundamental Research Funds for the Central Universities of Central South University (2014zzts015).

■ REFERENCES

(1) Chen, X.; Shen, S.; Guo, L.; Mao, S. S. Semiconductor-Based Photocatalytic Hydrogen Generation. *Chem. Rev.* **2010**, *110*, 6503−6570.
(2) Lu, Y.; Wang, D.; Yang, P.; Du, Y.; Lu, C. Coupling $Zn_xCd_{1-x}S$ Nanoparticles with Graphene-Like MoS_2: Superior Interfacial Contact, Low Overpotential and Enhanced Photocatalytic Activity under Visible-Light Irradiation. *Catal. Sci. Technol.* **2014**, *4*, 2650−2657.
(3) Zhou, H.; Qu, Y.; Zeid, T.; Duan, X. Towards Highly Efficient Photocatalysts Using Semiconductor Nanoarchitectures. *Energy Environ. Sci.* **2012**, *5*, 6732−6743.
(4) Fujishima, A.; Honda, K. Electrochemical Photolysis of Water at a Semiconductor Electrode. *Nature* **1972**, *238*, 37−38.
(5) Sun, W.-T.; Yu, Y.; Pan, H.-Y.; Gao, X.-F.; Chen, Q.; Peng, L.-M. CdS Quantum Dots Sensitized TiO_2 Nanotube-Array Photoelectrodes. *J. Am. Chem. Soc.* **2008**, *130*, 1124−1125.
(6) Liu, M.; Nam, C.-Y.; Black, C. T.; Kamcev, J.; Zhang, L. Enhancing Water Splitting Activity and Chemical Stability of Zinc Oxide Nanowire Photoanodes with Ultrathin Titania Shells. *J. Phys. Chem. C* **2013**, *117*, 13396−13402.
(7) Wolcott, A.; Smith, W. A.; Kuykendall, T. R.; Zhao, Y.; Zhang, J. Z. Photoelectrochemical Study of Nanostructured ZnO Thin Films for Hydrogen Generation from Water Splitting. *Adv. Funct. Mater.* **2009**, *19*, 1849−1856.
(8) Li, J.; Cushing, S. K.; Zheng, P.; Meng, F.; Chu, D.; Wu, N. Plasmon-Induced Photonic and Energy-Transfer Enhancement of Solar Water Splitting by a Hematite Nanorod Array. *Nat. Commun.* **2013**, *4*, 2651.
(9) Hodes, G.; Cahen, D.; Manassen, J. Tungsten Trioxide as a Photoanode for a Photoelectrochemical Cell (PEC). *Nature* **1976**, *260*, 312−313.
(10) Liu, X.; Wang, F.; Wang, Q. Nanostructure-Based WO_3 Photoanodes for Photoelectrochemical Water Splitting. *Phys. Chem. Chem. Phys.* **2012**, *14*, 7894−7911.
(11) Zheng, H.; Ou, J. Z.; Strano, M. S.; Kaner, R. B.; Mitchell, A.; Kalantar-zadeh, K. Nanostructured Tungsten Oxide-Properties, Synthesis, and Applications. *Adv. Funct. Mater.* **2011**, *21*, 2175−2196.
(12) Hsiao, P.-T.; Chen, L.-C.; Li, T.-L.; Teng, H. Vapor Treatment of Nanocrystalline WO_3 Photoanodes for Enhanced Photoelectrochemical Performance in the Decomposition of Water. *J. Mater. Chem.* **2011**, *21*, 19402.
(13) Zheng, H.; Tachibana, Y.; Kalantar-zadeh, K. Dye-Sensitized Solar Cells Based on WO_3. *Langmuir* **2010**, *26*, 19148−19152.
(14) Zhu, J.; Li, W.; Li, J.; Li, Y.; Hu, H.; Yang, Y. Photoelectrochemical Activity of $NiWO_4/WO_3$ Heterojunction Photoanode under Visible Light Irradiation. *Electrochim. Acta* **2013**, *112*, 191−198.
(15) Amano, F.; Tian, M.; Wu, G.; Ohtani, B.; Chen, A. Facile Preparation of Platelike Tungsten Oxide Thin Film Electrodes with High Photoelectrode Activity. *ACS Appl. Mater. Interfaces* **2011**, *3*, 4047−4052.
(16) Qin, D.-D.; Tao, C.-L.; Friesen, S. A.; Wang, T.-H.; Varghese, O. K.; Bao, N.-Z.; Yang, Z.-Y.; Mallouk, T. E.; Grimes, C. A. Dense Layers of Vertically Oriented WO_3 Crystals as Anodes for Photoelectrochemical Water Oxidation. *Chem. Commun.* **2012**, *48*, 729−731.
(17) Li, W.; Liu, C.; Yang, Y.; Li, J.; Chen, Q.; Liu, F. Platelike WO_3 from Hydrothermal RF Sputtered Tungsten Thin Films for Photoelectrochemical Water Oxidation. *Mater. Lett.* **2012**, *84*, 41−43.
(18) Su, J.; Feng, X.; Sloppy, J. D.; Guo, L.; Grimes, C. A. Vertically Aligned WO_3 Nanowire Arrays Grown Directly on Transparent Conducting Oxide Coated Glass: Synthesis and Photoelectrochemical Properties. *Nano Lett.* **2011**, *11*, 203−208.
(19) Kalanur, S. S.; Hwang, Y. J.; Chae, S. Y.; Joo, O. S. Facile Growth of Aligned WO_3 Nanorods on FTO Substrate for Enhanced Photoanodic Water Oxidation Activity. *J. Mater. Chem. A* **2013**, *1*, 3479.
(20) Zhu, K.; Neale, N. R.; Miedaner, A.; Frank, A. J. Enhanced Charge-Collection Efficiencies and Light Scattering in Dye-Sensitized Solar Cells Using Oriented TiO_2 Nanotubes Arrays. *Nano Lett.* **2006**, *7*, 69−74.
(21) Liu, B.; Aydil, E. S. Growth of Oriented Single-Crystalline Rutile TiO_2 Nanorods on Transparent Conducting Substrates for Dye-Sensitized Solar Cells. *J. Am. Chem. Soc.* **2009**, *131*, 3985−3990.
(22) Amano, F.; Li, D.; Ohtani, B. Photoelectrochemical Property of Tungsten Oxide Films of Vertically Aligned Flakes for Visible-Light-Induced Water Oxidation. *J. Electrochem. Soc.* **2011**, *158*, K42−K46.
(23) Muskens, O. L.; Rivas, J. G.; Algra, R. E.; Bakkers, E. P. A. M.; Lagendijk, A. Design of Light Scattering in Nanowire Materials for Photovoltaic Applications. *Nano Lett.* **2008**, *8*, 2638−2642.
(24) Cole, B.; Marsen, B.; Miller, E.; Yan, Y.; Jones, B.; Al-Jassim, K. M., Evaluation of Nitrogen Doping of Tungsten Oxide for Photoelectrochemical Water Splitting. *J. Phys. Chem. C* **2008**, *112*, 5213−5220.
(25) Cai, G.-f.; Wang, X.-l.; Zhou, D.; Zhang, J.-h.; Xiong, Q.-q.; Gu, C.-d.; Tu, J.-p. Hierarchical Structure Ti-Doped WO_3 Film with Improved Electrochromism in Visible-Infrared Region. *RSC Adv.* **2013**, *3*, 6896.
(26) Han, S.; Li, J.; Chen, X.; Huang, Y.; Liu, C.; Yang, Y.; Li, W. Enhancing Photoelectrochemical Activity of Nanocrystalline WO_3 Electrodes by Surface Tuning with Fe(III). *Int. J. Hydrogen Energy* **2012**, *37*, 16810−16816.
(27) Sun, Y.; Murphy, C. J.; Reyes-Gil, K. R.; Reyes-Garcia, E. A.; Thornton, J. M.; Morris, N. A.; Raftery, D. Photoelectrochemical and Structural Characterization of Carbon-Doped WO_3 Films Prepared via Spray Pyrolysis. *Int. J. Hydrogen Energy* **2009**, *34*, 8476−8484.
(28) Li, W.; Li, J.; Wang, X.; Chen, Q. Preparation and Water-Splitting Photocatalytic Behavior of S-Doped WO_3. *Appl. Surf. Sci.* **2012**, *263*, 157−162.
(29) Nah, Y. C.; Paramasivam, I.; Hahn, R.; Shrestha, N. K.; Schmuki, P. Nitrogen Doping of Nanoporous WO_3 Layers by NH_3 Treatment

for Increased Visible Light Photoresponse. *Nanotechnology* **2010**, *21*, 105704.

(30) Liu, Y.; Li, Y.; Li, W.; Han, S.; Liu, C. Photoelectrochemical Properties and Photocatalytic Activity of Nitrogen-Doped Nanoporous WO_3 Photoelectrodes under Visible Light. *Appl. Surf. Sci.* **2012**, *258*, 5038−5045.

(31) Shi, X.; Choi, I. Y.; Zhang, K.; Kwon, J.; Kim, D. Y.; Lee, J. K.; Oh, S. H.; Kim, J. K.; Park, J. H. Efficient Photoelectrochemical Hydrogen Production from Bismuth Vanadate-Decorated Tungsten Trioxide Helix Nanostructures. *Nat. Commun.* **2014**, *5*, 4775.

(32) Rao, P. M.; Cai, L.; Liu, C.; Cho, I. S.; Lee, C. H.; Weisse, J. M.; Yang, P.; Zheng, X. Simultaneously Efficient Light Absorption and Charge Separation in $WO_3/BiVO_4$ Core/Shell Nanowire Photoanode for Photoelectrochemical Water Oxidation. *Nano Lett.* **2014**, *14*, 1099−105.

(33) Li, H.; Zhou, Y.; Chen, L.; Luo, W.; Xu, Q.; Wang, X.; Xiao, M.; Zou, Z. Rational and Scalable Fabrication of High-Quality WO_3/CdS Core/Shell Nanowire Arrays for Photoanodes toward Enhanced Charge Separation and Transport under Visible Light. *Nanoscale* **2013**, *5*, 11933−9.

(34) Wang, G.; Yang, X.; Qian, F.; Zhang, J. Z.; Li, Y. Double-Sided CdS and CdSe Quantum Dot Co-Sensitized Zno Nanowire Arrays for Photoelectrochemical Hydrogen Generation. *Nano Lett.* **2010**, *10*, 1088−92.

(35) Lee, Y.-L.; Chi, C.-F.; Liau, S.-Y. CdS/CdSe Co-Sensitized TiO_2 Photoelectrode for Efficient Hydrogen Generation in a Photoelectrochemical Cell. *Chem. Mater.* **2010**, *22*, 922−927.

(36) Liu, C.; Li, Y.; Li, W.; Zhu, J.; Li, J.; Chen, Q.; Yang, Y. CdS Quantum Dots Sensitized Platelike WO_3 Photoelectrodes with a TiO_2 Buffer-Layer. *Mater. Lett.* **2014**, *120*, 170−173.

(37) Brennan, T. P.; Trejo, O.; Roelofs, K. E.; Xu, J.; Prinz, F. B.; Bent, S. F. Efficiency Enhancement of Solid-State PbS Quantum Dot-Sensitized Solar Cells with Al_2O_3 Barrier Layer. *J. Mater. Chem. A* **2013**, *1*, 7566.

(38) Chai, B.; Peng, T.; Zeng, P.; Mao, J. Synthesis of Floriated In_2S_3 Decorated with TiO_2 Nanoparticles for Efficient Photocatalytic Hydrogen Production under Visible Light. *J. Mater. Chem.* **2011**, *21*, 14587.

(39) Zeng, Q.; Bai, J.; Li, J.; Li, Y.; Li, X.; Zhou, B. Combined Nanostructured Bi_2S_3/TNA Photoanode and Pt/SiPVC Photocathode for Efficient Self-Biasing Photoelectrochemical Hydrogen and Electricity Generation. *Nano Energy* **2014**, *9*, 152−160.

(40) Tahir, A. A.; Ehsan, M. A.; Mazhar, M.; Wijayantha, K. G. U.; Zeller, M.; Hunter, A. D. Photoelectrochemical and Photoresponsive Properties of Bi_2S_3 Nanotube and Nanoparticle Thin Films. *Chem. Mater.* **2010**, *22*, 5084−5092.

(41) Bao, N.; Shen, L.; Takata, T.; Domen, K.; Gupta, A.; Yanagisawa, K.; Grimes, C. A. Facile Cd−Thiourea Complex Thermolysis Synthesis of Phase-Controlled CdS Nanocrystals for Photocatalytic Hydrogen Production under Visible Light. *J. Phys. Chem. C* **2007**, *111*, 17527−17534.

(42) Franco, A.; Neves, M. C.; Carrott, M. M. L. R.; Mendonça, M. H.; Pereira, M. I.; Monteiro, O. C. Photocatalytic Decolorization of Methylene Blue in the Presence of TiO_2/ZnS Nanocomposites. *J. Hazard. Mater.* **2009**, *161*, 545−550.

(43) Hu, J.-S.; Ren, L.-L.; Guo, Y.-G.; Liang, H.-P.; Cao, A.-M.; Wan, L.-J.; Bai, C.-L. Mass Production and High Photocatalytic Activity of ZnS Nanoporous Nanoparticles. *Angew. Chem.* **2005**, *117*, 1295−1299.

(44) Xie, S.; Lu, X.; Zhai, T.; Gan, J.; Li, W.; Xu, M.; Yu, M.; Zhang, Y. M.; Tong, Y. Controllable Synthesis of $Zn_xCd_{1-X}S$@ZnO Core-Shell Nanorods with Enhanced Photocatalytic Activity. *Langmuir* **2012**, *28*, 10558−64.

(45) Reber, J. F.; Rusek, M. Photochemical Hydrogen Production with Platinized Suspensions of Cadmium Sulfide and Cadmium Zinc Sulfide Modified by Silver Sulfide. *J. Phys. Chem.* **1986**, *90*, 824−834.

(46) Santra, P. K.; Kamat, P. V. Mn-Doped Quantum Dot Sensitized Solar Cells: A Strategy to Boost Efficiency over 5%. *J. Am. Chem. Soc.* **2012**, *134*, 2508−11.

(47) Gakhar, R.; Merwin, A.; Summers, K.; Pilli, S. K.; Chidambaram, D. Application of $Zn_xCd_{1-X}Se$-Sensitized TiO_2 Nanotube Arrays as Photoanodes for Solar Cells. *J. Mater. Chem. A* **2014**, *2*, 10116.

(48) Yang, J.; Li, W.; Li, J.; Sun, D.; Chen, Q. Hydrothermal Synthesis and Photoelectrochemical Properties of Vertically Aligned Tungsten Trioxide (Hydrate) Plate-Like Arrays Fabricated Directly on FTO Substrates. *J. Mater. Chem.* **2012**, *22*, 17744.

(49) Liu, Y.; Li, W.; Li, J.; Yang, Y.; Chen, Q. Enhancing Photoelectrochemical Performance with a Bilayer-Structured Film Consisting of Graphene−WO_3 Nanocrystals and WO_3 Vertically Plate-Like Arrays as Photoanodes. *RSC Adv.* **2014**, *4*, 3219.

(50) Koh, Y. W.; Lai, C. S.; Du, A. Y.; Tiekink, E. R. T.; Loh, K. P. Growth of Bismuth Sulfide Nanowire Using Bismuth Trisxanthate Single Source Precursors. *Chem. Mater.* **2003**, *15*, 4544−4554.

(51) Zhao, Y.; Chua, K. T. E.; Gan, C. K.; Zhang, J.; Peng, B.; Peng, Z.; Xiong, Q. Phonons in Bi_2S_3 Nanostructures: Raman Scattering and First-Principles Studies. *Phys. Rev. B* **2011**, *84*, 205330.

(52) Trentelman, K. A Note on the Characterization of Bismuth Black by Raman Microspectroscopy. *J. Raman Spectrosc.* **2009**, *40*, 585−589.

(53) Yang, L.; Zhou, R.; Lan, J.; Zhang, Q.; Cao, G.; Zhu, J. Efficient Band Alignment for $Zn_xCd_{1-X}Se$ QD-Sensitized TiO_2 Solar Cells. *J. Mater. Chem. A* **2014**, *2*, 3669.

(54) He, H.; Berglund, S. P.; Xiao, P.; Chemelewski, W. D.; Zhang, Y.; Mullins, C. B. Nanostructured Bi_2S_3/WO_3 Heterojunction Films Exhibiting Enhanced Photoelectrochemical Performance. *J. Mater. Chem. A* **2013**, *1*, 12826.

(55) Miao, X.; Pan, K.; Liao, Y.; Zhou, W.; Pan, Q.; Tian, G.; Wang, G. Controlled Synthesis of Mesoporous Anatase TiO_2 Microspheres as a Scattering Layer to Enhance the Photoelectrical Conversion Efficiency. *J. Mater. Chem. A* **2013**, *1*, 9853−9861.

(56) Wang, F.; Wang, Y.; Zhan, X.; Safdar, M.; Gong, J.; He, J.; Nanoparticle, Pt and CdS Quantum Dot Assisted WO_3 Nanowires Grown on Flexible Carbon Fibers for Efficient Oxygen Production. *CrystEngComm* **2014**, *16*, 1389.

(57) Zha, C.; Shen, L.; Zhang, X.; Wang, Y.; Korgel, B. A.; Gupta, A.; Bao, N. Double-Sided Brush-Shaped TiO2 Nanostructure Assemblies with Highly Ordered Nanowires for Dye-Sensitized Solar Cells. *ACS. Appl. Mater. Interfaces* **2014**, *6*, 122−9.

(58) Su, J.; Feng, X.; Sloppy, J. D.; Guo, L.; Grimes, C. A. Vertically Aligned WO_3 Nanowire Arrays Grown Directly on Transparent Conducting Oxide Coated Glass: Synthesis and Photoelectrochemical Properties. *Nano Lett.* **2011**, *11*, 203−8.

(59) Su, J.; Guo, L.; Bao, N.; Grimes, C. A. Nanostructured $WO_3/BiVO_4$ Heterojunction Films for Efficient Photoelectrochemical Water Splitting. *Nano Lett.* **2011**, *11*, 1928−33.

(60) Rath, A. K.; Bernechea, M.; Martinez, L.; Konstantatos, G. Solution-Processed Heterojunction Solar Cells Based on p-Type PbS Quantum Dots and n-Type Bi_2S_3 Nanocrystals. *Adv. Mater.* **2011**, *23*, 3712−7.

(61) Zhang, Z.; Wang, W.; Wang, L.; Sun, S. Enhancement of Visible-Light Photocatalysis by Coupling with Narrow-Band-Gap Semiconductor: a Case Study on Bi_2S_3/Bi_2WO_6. *ACS. Appl. Mater. Interfaces* **2012**, *4*, 593−7.

(62) Wang, Y.; Wang, Y.; Xu, R. Synthesis of Zn−Cu−Cd Sulfide Nanospheres with Controlled Copper Locations and Their Effects on Photocatalytic Activities for H_2 Production. *Int. J. Hydrogen Energy* **2010**, *35*, 5245−5253.

(63) Wu, Z.; Chen, L.; Xing, C.; Jiang, D.; Xie, J.; Chen, M. Controlled Synthesis of Bi_2S_3/ZnS Microspheres by an in Situ Ion-Exchange Process with Enhanced Visible Light Photocatalytic Activity. *Dalton Trans.* **2013**, *42*, 12980−8.

(64) Robert, D. Photosensitization of TiO_2 by M_xO_y and M_xS_y Nanoparticles for Heterogeneous Photocatalysis Applications. *Catal. Today* **2007**, *122*, 20−26.

DOI: 10.1021/acsami.5b00830
ACS Appl. Mater. Interfaces 2015, 7, 10763−10770